**DESIGN OF A BALANCED MICROSTRIP
FILTER**

J.W. Bandler, M.H. Bakr, C.E. Falt and N. Georgieva

SOS-99-16-R

June 1999

DESIGN OF A BALANCED MICROSTRIP LINE FILTER

J.W. Bandler, M.H. Bakr, C.E. Falt and N. Georgieva

Abstract

In this work we discuss the design of a Balanced Microstrip Filter (BMF). This filter is operated in the odd mode to reduce radiation losses. The filter is simulated through Sonnet's ***em***. This design is time-intensive. We utilized the efficient Hybrid Aggressive Space Mapping (HASM) algorithm. A coarse model that uses empirical models of coupled microstrip lines and Walker's formulas is utilized. The algorithm managed to align the optimal coarse model response and the fine model response. However, the final design is not as good as the one obtained by direct optimization. We carried out a convergence analysis of the simulator behavior. We show that simulator inaccuracy is the main reason for the HASM algorithm to stop prematurely.

M.H. Bakr, J.W. Bandler and N. Georgieva are with the Simulation Optimization Systems Research Laboratory and the Department of Electrical and Computer Engineering, McMaster University, Hamilton, Ontario, Canada, L8S 4K1.

J.W. Bandler is also with Bandler Corporation, P.O. Box 8083, Dundas, Ontario, Canada L9H 5E7.

C.E. Falt is with Advanced High Speed Projects, Nortel Networks, P.O.Box 3511 Station C, Ottawa, Canada K1Y 4H7.

I. INTRODUCTION

The design of a balanced microstrip filter (BMF) using the Hybrid Aggressive Space Mapping (HASM) algorithm [1, 2] is presented in this report. The design is based on a structure proposed by Chris Falt in 1996 [3] (see Fig. 1). It alleviates one of the major shortcomings of microstrip filters, namely, their excessive radiation loss at frequencies higher than 20 GHz. It uses open-end coupled microstrip line sections operating in odd mode. Due to the odd mode, the field is very much concentrated in the slot between the microstrip lines of each balanced section, thus significantly restricting the excitation of surface waves or the radiation from the open ends of the microstrip coupled lines.

In a previous work [4], direct optimization of the BMF was carried out. It has been already established that the design of the BMF is very troublesome due to three main factors. First, the empirical formulas used to build the equivalent circuit are not accurate at the frequency band of operation 27 GHz $\leq f \leq 29$ GHz. As a result, the equivalent circuit can be used only for approximate evaluation [4]. Second, the structure is very sensitive to changes of all optimized lengths l_{in}, l_{s1}, l_{s2}, l_{clb} and l_{cln} and a very fine mesh size <0.5 mil along the *x*-axis (see Fig. 1) is recommended for the fine model to be trusted within an error of 10%. Unfortunately, this would require several hours of simulation time per frequency sweep, which would make a direct optimization impractical. Third, the optimization problem is additionally complicated by multiple minima.

The HASM algorithm offers an opportunity to fully automate the otherwise extremely cumbersome conventional design procedure. It requires the existence of a coarse model for the circuit under consideration. Here, we utilize the equivalent circuit developed in [4], which modeled the coupling between microstrip lines through the empirical formulas suggested by Walker [5, 6]. This model is not accurate but was used in [4] to obtain a reasonable starting point for the direct optimization of a fine electromagnetic (EM) model. On the other hand, it is an excellent candidate for a Space Mapping coarse model [1, 2].

The HASM algorithm managed to successfully align the two responses. However, the final design slightly violates the design specifications.

The difficulties faced in the direct optimization [4] and the premature termination of the HASM algorithm prompted us to carry out a convergence analysis of the EM simulator. The results of the convergence analysis are discussed later in this report. They confirm the recommendation made in [4] of setting a fine mesh size <0.5 mil along the *x*-axis for a reliable calculation of the filter response and its derivatives with respect to the optimized parameters.

We start by describing the filter structure and design specifications in Section II. The utilized coarse model is then described in Section III. Also the design of this coarse model is discussed. The HASM optimization of the balanced filter is discussed in Section IV. The convergence analysis of the simulator is discussed in Section V. Finally, the conclusions are given in Section VI.

II. STRUCTURE DESCRIPTION AND DESIGN SPECIFICATIONS

The BMF is shown in Fig. 1. This figure shows that the filter is characterized by eight parameters: w, s_0, s_c, l_{in}, l_{s1}, l_{s2}, l_{clb} and l_{cln}. We keep w, s_0 and s_c fixed at 5.0 mils each. The design specifications for this problem are

$$|S_{21}| \geq 0.987 \text{ (-0.108 dB) for } 27.625 \text{ GHz} \leq f \leq 28.375 \text{ GHz} \tag{1}$$

and

$$|S_{21}| \leq 0.25 \text{ for } f \leq 27.2 \text{ GHz and } f \geq 28.8 \text{ GHz} \tag{2}$$

The relative bandwidth for these design constraints is 2.68 %. The port impedance at both differential ports is Z_0=100 Ω. The ports of the filter are operated in the odd mode (balanced excitation). The main advantage of the balanced filters is the reduction of radiation losses at millimeter wavelengths. A balun structure may be used to connect the ports of the balanced filter to the line feed to provide the necessary phase shift at the ports. The substrate has a height of h=10 mil and a relative dielectric constant of e_r=2.2.

III. THE COARSE MODEL

The coarse model is an equivalent circuit, which uses the built-in coupled microstrip-line model

of OSA90/hope [7] and Walker's formulas [5, 6] to represent the four-line sections of the filter. The netlist file for this model is given in Appendix A. To understand the model better, the following guidelines can be given. The filter includes four four-line sections, which are two by two identical with lengths l_{s1} and l_{s2}, respectively. Besides, it includes three coupled microstrip-line sections. Two of the microstrip-coupled lines are identical with a length of l_{clb}, and the other one has a length of l_{cln} (see Fig. 1). The two four-line sections are defined as a subcircuits in the netlist file: c_lines_1 and c_lines_2. The difference between them is only in their length. An example geometry of a four-line microstrip section is given in Fig. 2. The corresponding equivalent circuit is given in Fig. 3.

It is important to mention that this equivalent circuit is relevant to the odd-mode case, where push-pull feed is applied at ports 1-4, 2-3, 5-8 and at 6-7. Thus, the above equivalent circuit represents two coupled coupled-line sections operating in an odd mode. Note that only the inner coupling is represented via Walker's formulas, while the outer couplings are represented using the built-in microstrip coupled line model in OSA90/hope. This element notation is MSCL in OSA90/hope library.

The inductances L_m [H] and the capacitances C_m [F] are calculated by making use of the inductance per unit length L_{m1} [H/m] and the capacitance per unit length C_{m1} [F/m] of Walker's formulas [5, 6].

III. OPTIMIZATION OF THE COARSE MODEL

The first step in the HASM algorithm is to obtain an optimal design for the fast and less accurate coarse model. The coarse model is optimized to satisfy the design constraints (1) and (2). The starting point for optimization is given in Table I. The corresponding coarse model response is shown in Fig. 4.

The optimal coarse model design is given in Table I. The corresponding response is shown in Fig. 5. This design satisfies the optimization specifications with a maximum error of –0.0050606. The solution is not unique and it is established that at least two local minima represent good designs (exceeding the design specifications).

IV. HASM OPTIMIZATION

The fine model is the filter simulated by Sonnet's *em* [8] through Empipe [7]. The filter is first parameterized. The nominal geometry file is shown in Fig. 6. The nominal and perturbed values of the fine model parameters utilized in the parameterization process are given in Fig. 7.

Note that the mesh size alongside the filter (*x* axis) is 0.5 mil or 0.0127 mm. The choice of such a mesh size was dictated by the sensitivity of the responses with respect to the open-end microstrip-section lengths.

To make the design time-efficient we disabled the interpolation feature available in Empipe [7]. The starting point for the HASM algorithm is the optimal coarse model design snapped to the nearest on-grid point. This point is given in Table II. The corresponding fine model responses are given in Figs. 8, 9 and 10. These figures show that the significant misalignment between the optimal coarse model response and the fine model response.

Due to the sensitivity of the responses with respect to the optimizable parameters, the points used for the multi-point parameter extraction are within a fixed region that is smaller in size than the trust region utilized. The first phase of the HASM algorithm executed successfully two iterations that required 7 fine model simulations. The design at the end of the first phase x'_{em} is given in Table II. The corresponding responses are shown in Figs. 11, 12 and 13. These figures show that the first phase managed to shift the fine model response to the proper frequency band. The locations of the poles of the response are also close to their expected values. However, there is still significant reflection in the passband.

The mapping established in the first phase is utilized by the algorithm to get an estimate for the Jacobian of the fine model response. The algorithm then switches to the second phase which executed 10 successful iterations that required 13 fine model simulations. The design at the end of the second phase (x''_{em}) is given in Table II. The corresponding responses are shown in Figs. 14, 15 and 16. This design

has a better match to the optimal coarse model response. However, the design constraints are slightly violated.

The HASM algorithm defaults to minimax optimization to ensure optimality of the design. The starting point for the minimax optimizer is x''_{em}. The solution x^*_{em} is given in Table II. The corresponding responses are given in Figs. 17, 18 and 19. This design does not satisfy the design specifications. Minimax optimization reached a local minimum that is different from that reported in [4].

V. CONVERGENCE ANALYSIS

The difficulty encountered in the direct optimization [4] and the premature termination of the HASM algorithm prompted us to investigate the accuracy of the simulator. The size of the grid along the x-direction is made 0.25 mils while keeping the grid size along the y-direction constant. The S parameters at the on-grid point x''_{em} were obtained for the case Δx=0.25 mils. We then evaluated the complex difference between the S parameters at the on-grid point x''_{em} obtained using Δx=0.25 mils and Δx=0.5 mils. The modulus of this complex difference is shown in Fig. 20 for a complete frequency sweep. This figure shows that the modulus of the change in S_{21} can go up to 0.065. We believe that this high value of $|\Delta S|$ is the basic reason for the difficulty facing direct optimization (many local minima). Also, we believe it is the basic reason for the premature termination of the HASM algorithm.

We investigated the effect of the inaccuracy of the simulated responses on the derivatives of the objective function $L = \left\| R_{em}(x_{em}) - R_{os}(x^*_{os}) \right\|_2$ with respect to the two parameters l_{in} and l_{s1}. We chose to make this comparison at the on-grid point x''_{em}. The gradient is evaluated using both forward and backward differences for the cases Δx=0.5 mils and Δx=0.25 mils. For the case Δx=0.5 mils we have

$$
\begin{bmatrix} \dfrac{\partial L}{\partial l_{in}} \\ \dfrac{\partial L}{\partial l_{s1}} \end{bmatrix}_f = \begin{bmatrix} 0.0144 \\ 0.0138 \end{bmatrix} \quad \text{and} \quad \begin{bmatrix} \dfrac{\partial L}{\partial l_{in}} \\ \dfrac{\partial L}{\partial l_{s1}} \end{bmatrix}_b = \begin{bmatrix} 0.0168 \\ -0.2612 \end{bmatrix} \tag{3}
$$

6

and for $\Delta x = 0.25$ mils we have

$$\begin{bmatrix} \dfrac{\partial L}{\partial l_{in}} \\ \dfrac{\partial L}{\partial l_{s1}} \end{bmatrix}_f = \begin{bmatrix} 0.0152 \\ -0.0572 \end{bmatrix} \quad \text{and} \quad \begin{bmatrix} \dfrac{\partial L}{\partial l_{in}} \\ \dfrac{\partial L}{\partial l_{s1}} \end{bmatrix}_b = \begin{bmatrix} 0.0176 \\ -0.2144 \end{bmatrix} \tag{4}$$

Note that in (3) there is a difference in the sign and a significant difference in the magnitude (a factor of approximately 18.93) between the forward and the backward derivative with respect to the parameter l_{s1}. This signals unsuitable grid size due to high sensitivity with respect to this parameter. The change of sign may cause an optimization algorithm to assume that this point is a local minimum.

In (4) we notice that there is no difference in sign between the forward and backward derivative with respect to l_{s1}. However, there is still some difference in the magnitude. The derivatives in (4) show that the point x''_{em} can not be mistaken as a local minimum using the more accurate results obtained using $\Delta x = 0.25$ mils. The derivatives with respect to l_{in} are consistent in both (3) and (4).

We also investigated the accuracy of the design obtained through direct optimization in [4]. Figs. 21 and 22 show the response simulated using $\Delta x = 0.5$ mils and $\Delta x = 0.25$ mils, respectively. It is clear from these figures that the design specifications are satisfied in both cases. The complex difference between the S parameters for this design using $\Delta x = 0.5$ mils and $\Delta x = 0.25$ mils is calculated. Its modulus is shown in Fig. 23. It is clear that $|\Delta S_{11}|$ is small in the passband and this made the design still satisfy the specifications using the refined mesh.

The previous discussion recommends that a finer grid size (<0.5 mils) in the x-direction be used. However, using such a fine grid size makes the optimization process formidable due to the intensive time requirements.

VI. CONCLUSIONS

In this work we discussed the Hybrid Aggressive Space Mapping (HASM) optimization of a balanced microstrip filter. The coarse model utilizes empirical models for the coupled microstrip lines and Walker's formulas. The fine model utilizes Sonnet's *em*. The algorithm managed to considerably align the coarse and fine model responses. However, the final design still violates the design specifications. The premature termination of the algorithm and the difficulties reported in direct optimization prompted us to investigate the accuracy of the simulator. We showed that there is a considerable change in the *S*-parameters when a finer grid is utilized. The many local minima noticed during direct optimization and the premature termination of the HASM algorithm are mainly attributed to the accuracy of the simulator. The design is currently being refined by utilizing Sonnet's *em* simulation with a very fine mesh, and the HASM algorithm.

REFERENCES

[1]   J.W. Bandler, R.M. Biernacki, S.H. Chen, R.H. Hemmers and K. Madsen, "Electromagnetic optimization exploiting aggressive space mapping," *IEEE Trans. Microwave Theory Tech.*, vol. 43, 1995, pp. 2874-2882.

[2]   M.H. Bakr, J.W. Bandler, N. Georgieva and K. Madsen, "A hybrid aggressive space mapping algorithm for EM optimization," *IEEE MTT-S Int. Microwave Symp. Dig*. (Anaheim, CA), 1999.

[3]   C.E. Falt, Low Radiation Balanced Microstrip Bandpass Filter, *United States Patent*, Patent Number 5825263.

[4]   J.W. Bandler, M.H. Bakr, C.E. Falt and N. Georgieva, "Design of a balanced microstrip filter," Simulation Optimization Systems Research Laboratory, McMaster University, Hamilton, Canada, Report SOS-99-4-R, February 1999 (Revised June 1999).

[5]   C.S. Walker, *Capacitance, Inductance and Crosstalk Analysis*. Norwood, MA: Artech House, 1990.

[6]   J.W. Bandler and J.E. Rayas-Sánchez, "Interconnect crosstalk minimization: an alternative route," Simulation Optimization Systems Research Laboratory, McMaster University, Hamilton, Canada, Report SOS-98-8-R, April 1998, Appendix A.

[7]   OSA90/hope™ and Empipe™ Version 4.0, formerly Optimization Systems Associates Inc., P.O. Box 8083, Dundas, Ontario, Canada L9H 5E7, 1997, now HP EEsof Division, Hewlett-Packard Company, 1400 Fountaingrove Parkway, Santa Rosa, CA 95403-1799.

[8]   *em*™, Version 4.0b, Sonnet Software, Inc., 1020 Seventh North Street, Suite 210, Liverpool, NY 13088, 1997.

TABLE I
THE INITIAL AND OPTIMAL DESIGN OF
THE COARSE MODEL

Parameter	Initial value	Optimal value
l_{in}	50	77.1561
l_{s1}	50	42.5598
l_{s2}	7.2	8.81322
l_{clb}	100	103.850
l_{cln}	147	146.651

All values are in mils

TABLE II
THE OPTIMAL COARSE MODEL DESIGN AND THE DESIGNS
OBTAINED DURING DIFFERENT PHASES OF THE HASM ALGORITHM

Parameter	x^*_{os} (snapped)	x'_{em}	x''_{em}	x^*_{em}
l_{in}	77.0	65.5	54.0	49.1348
l_{s1}	42.5	52.5	53.5	50.5811
l_{s2}	9.0	7.0	7.0	7.0000
l_{clb}	104.0	97.0	96.5	99.5590
l_{cln}	147.0	147.0	147.0	147.493

All values are in mils

10
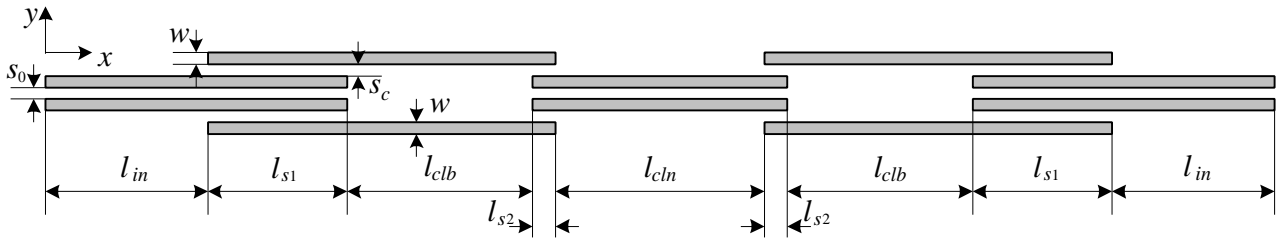
Fig. 1. The balanced microstrip filter.
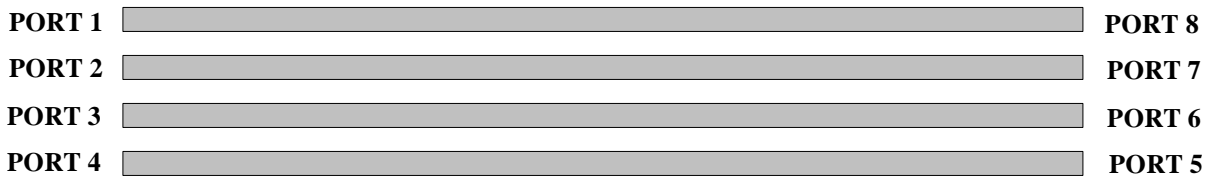
Fig. 2. Four coupled microstrip-line section.
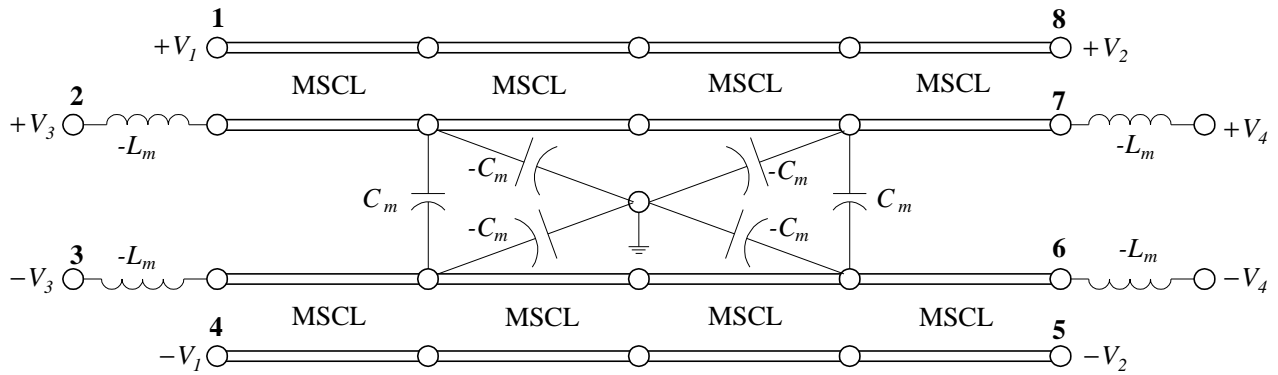
Fig. 3. Equivalent circuit used as a very coarse approximation of a section of two coupled coupled-microstrip lines.
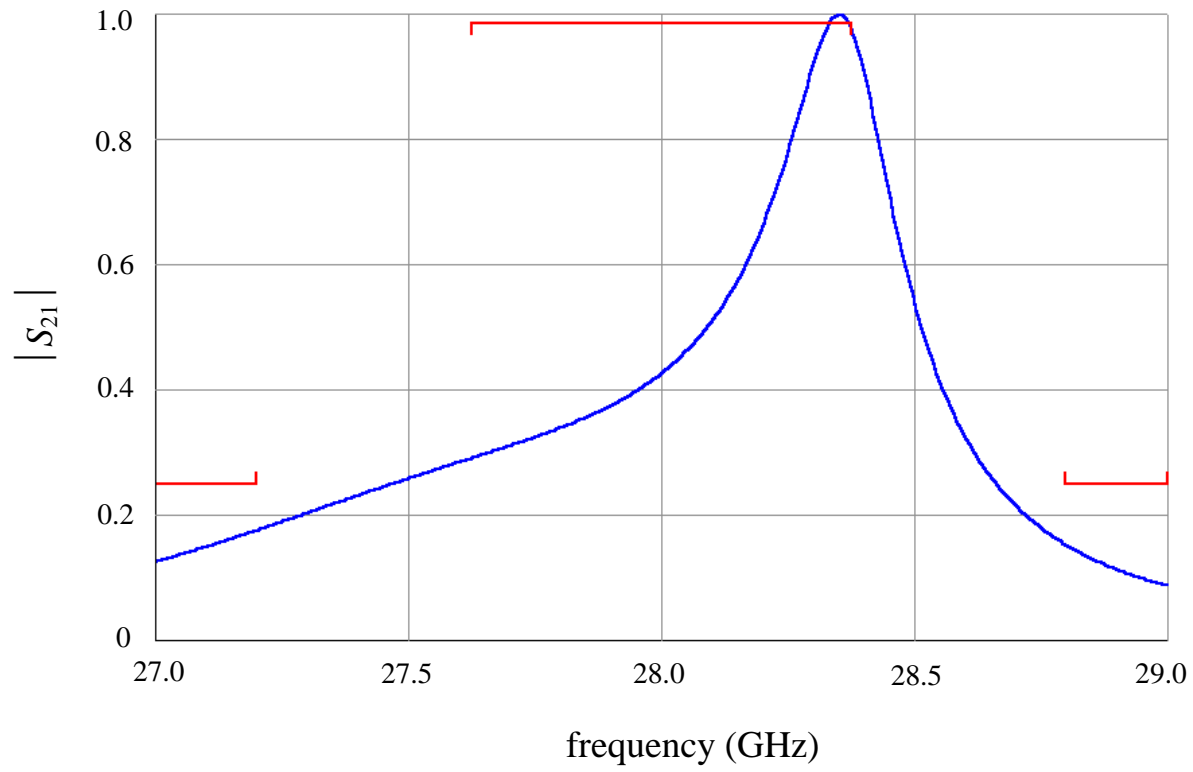
Fig. 4. The coarse model response at the starting point.
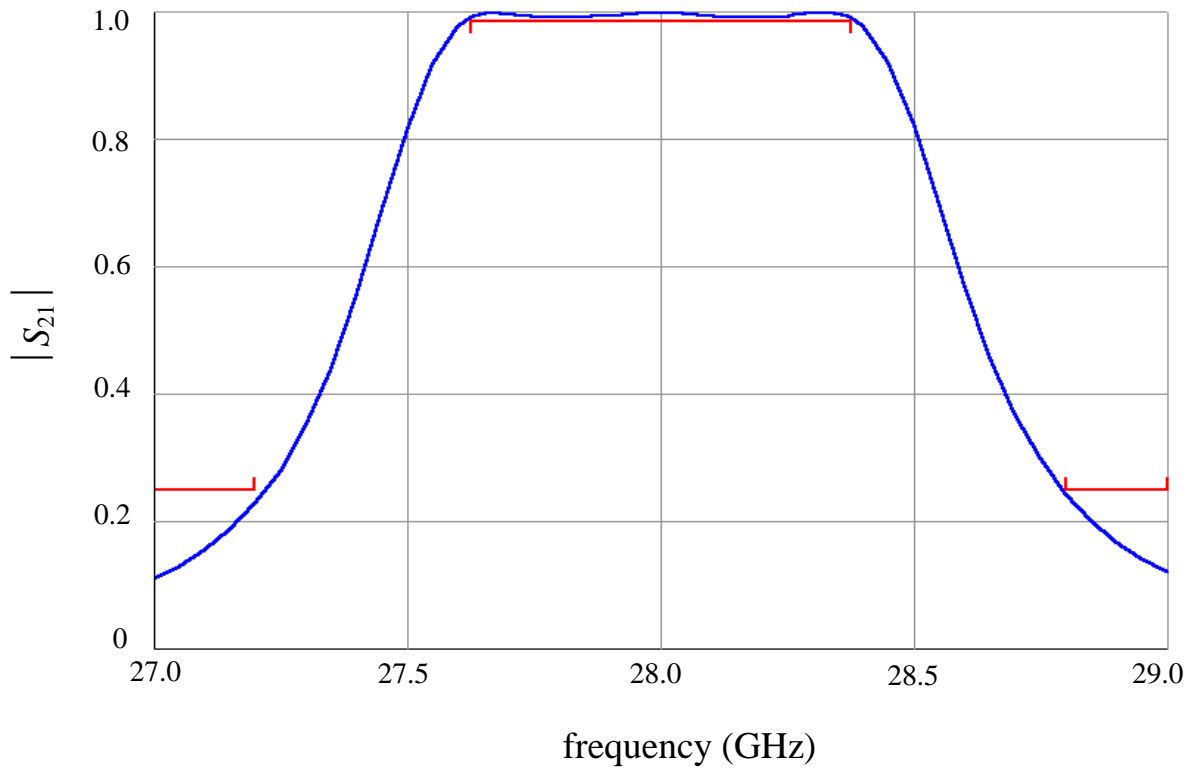
Fig. 5. The optimal coarse model response.
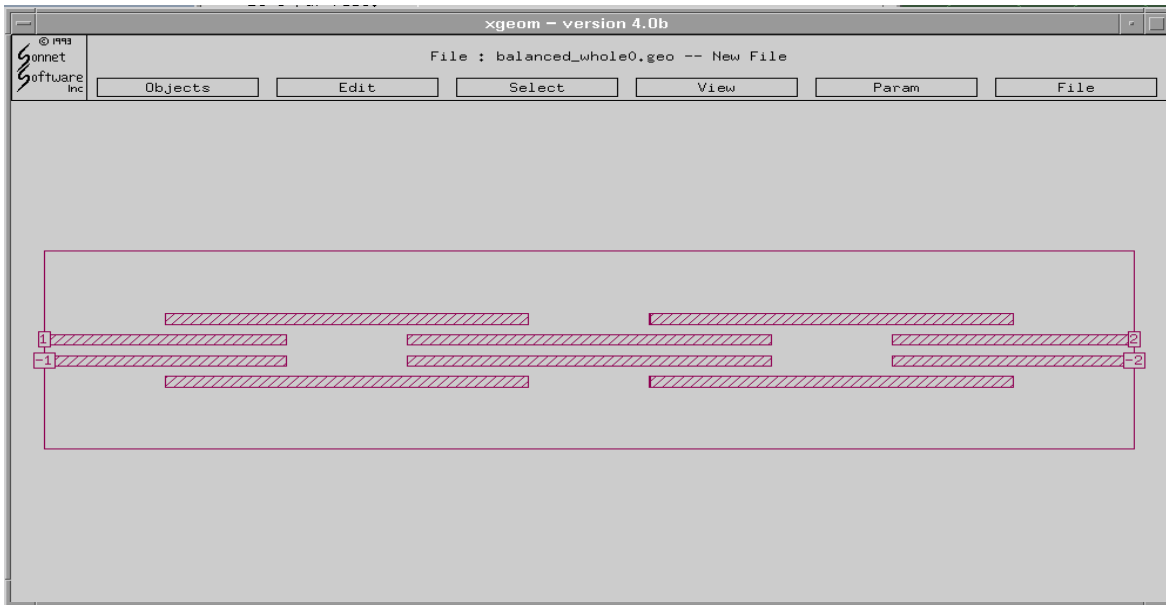
Fig. 6. The nominal geometry file used for the geometry capture of the fine model.
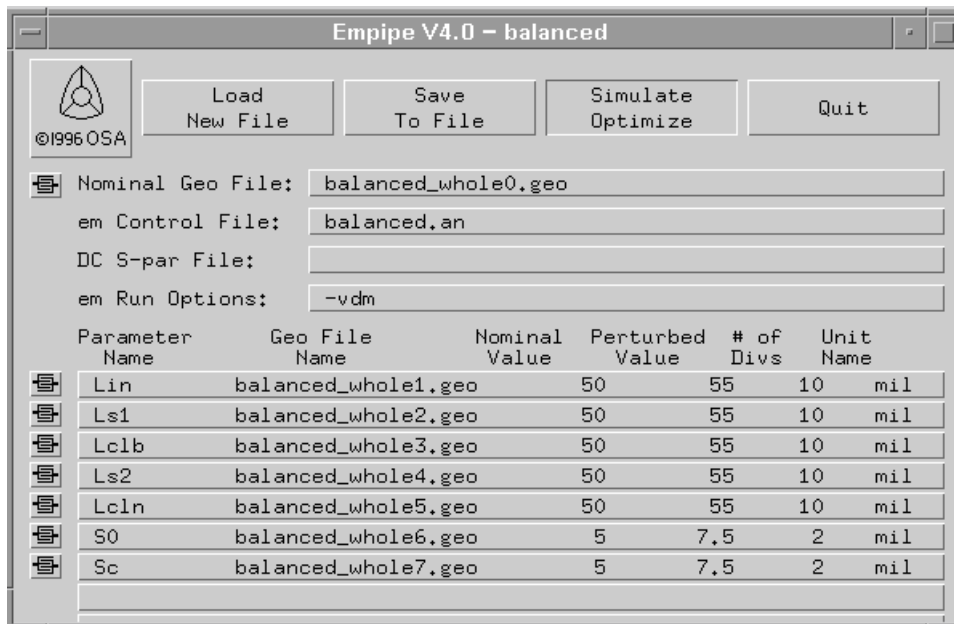
Fig. 7. Nominal and perturbed values of the optimized parameters in the fine model.

13
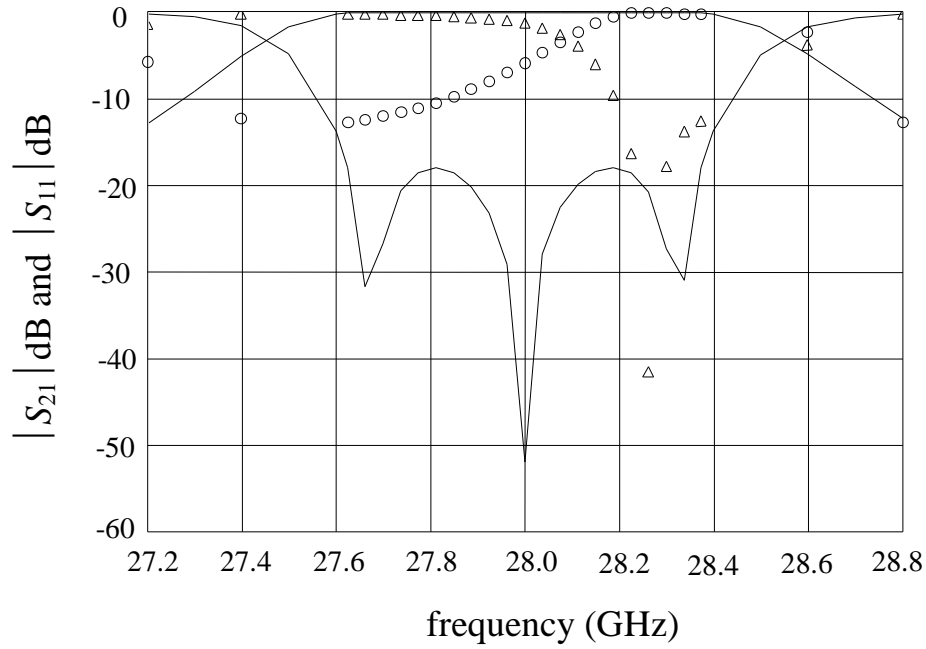
Fig. 8. The optimal coarse model response (—) (both $|S_{11}|$ and $|S_{21}|$) and the initial fine model response ($|S_{21}|$ (o) and $|S_{11}|$ (Δ)).
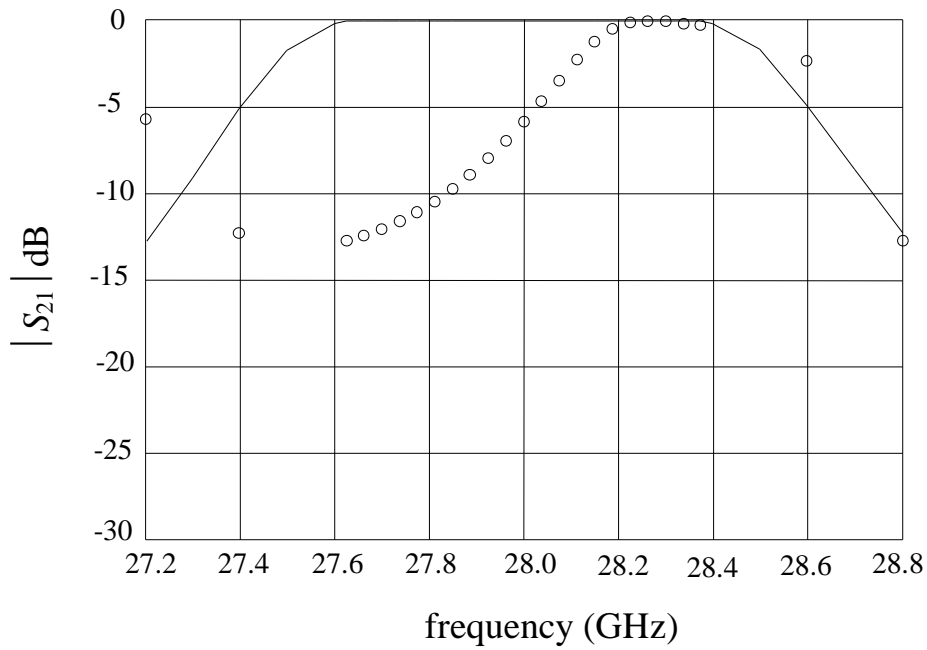
Fig. 9. The optimal coarse model response (—) and the initial fine model response (o).

14
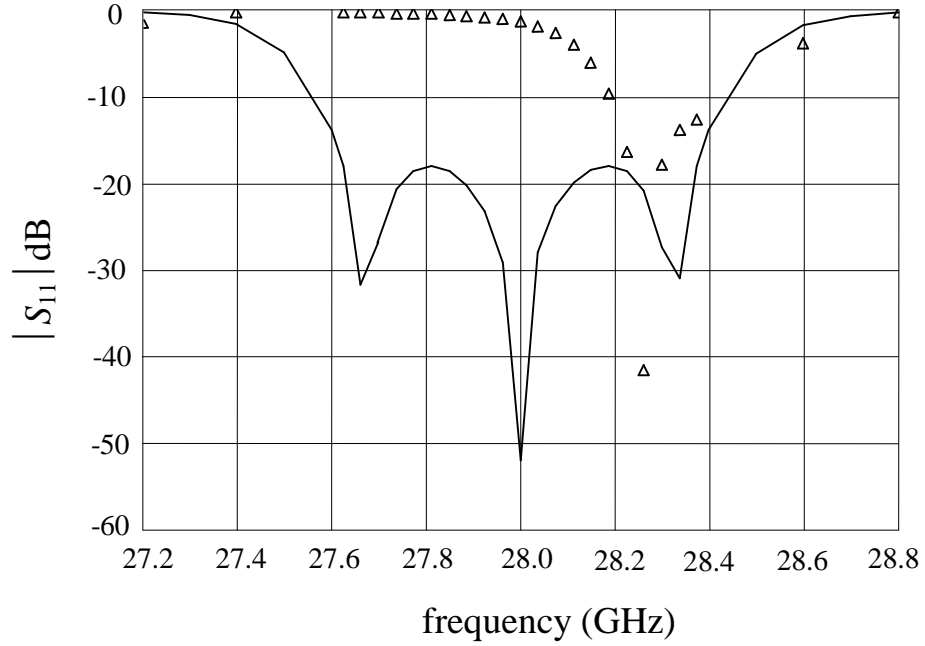
Fig. 10. The optimal coarse model response (—) and the initial fine model response (Δ).
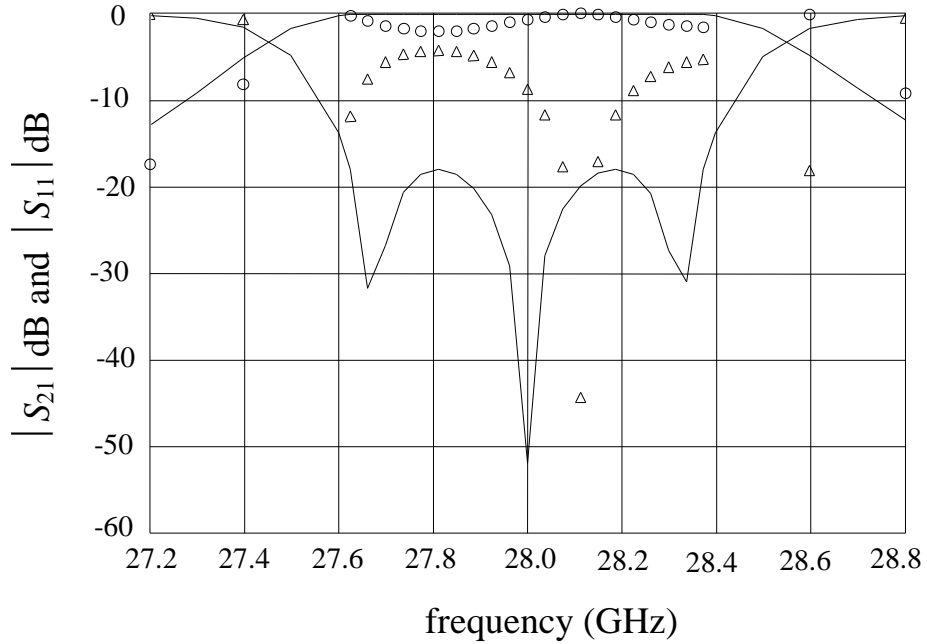
Fig. 11. The optimal coarse model response (—) (both $|S_{11}|$ and $|S_{21}|$) and the fine model response at the end of the first phase ($|S_{21}|$ (o) and $|S_{11}|$ (Δ)).
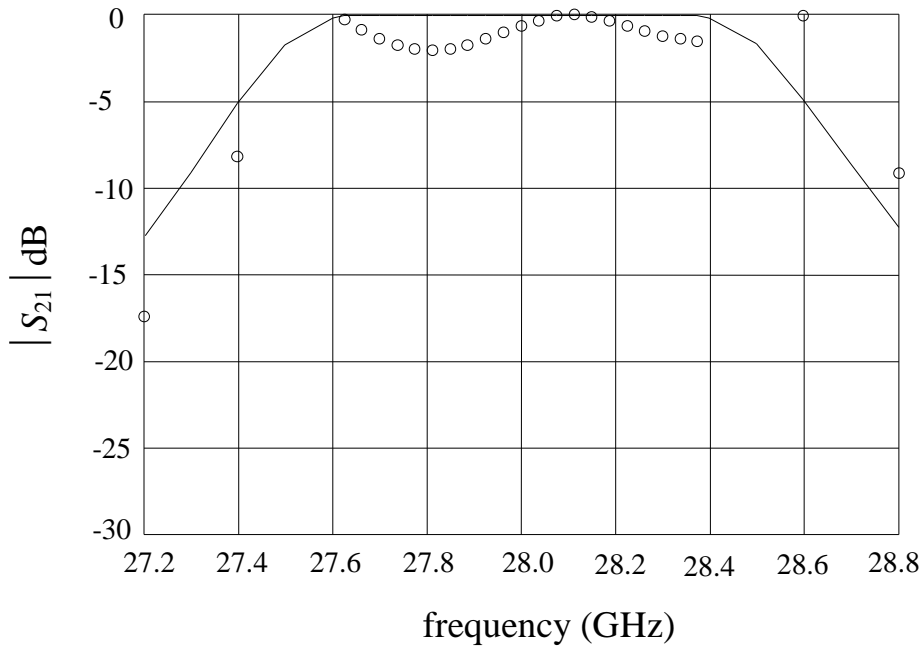
Fig. 12. The optimal coarse model response (——) and the fine model response (o) at the end of the first phase.
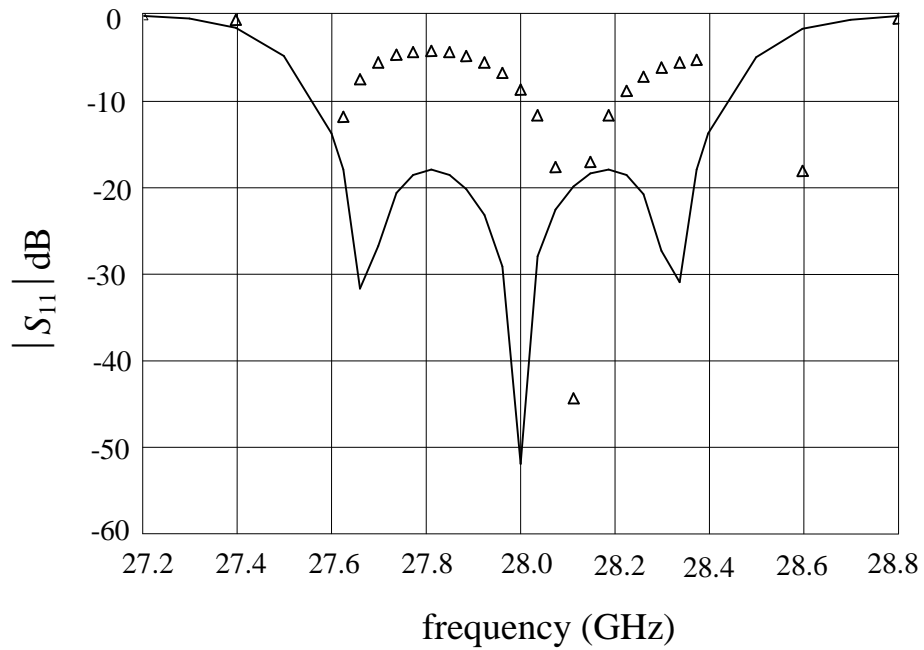
Fig. 13. The optimal coarse model response (——) and the fine model response (Δ) at the end of the first phase.

16
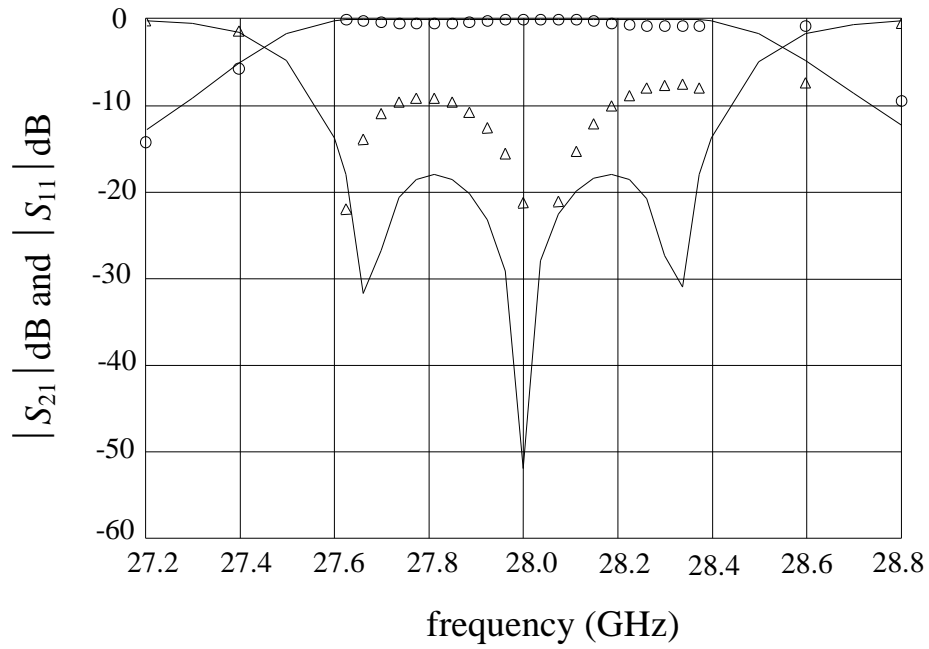
Fig. 14. The optimal coarse model response (—) (both $|S_{11}|$ and $|S_{21}|$) and the fine model response at the end of the second phase ($|S_{21}|$ (o) and $|S_{11}|$ (Δ)).
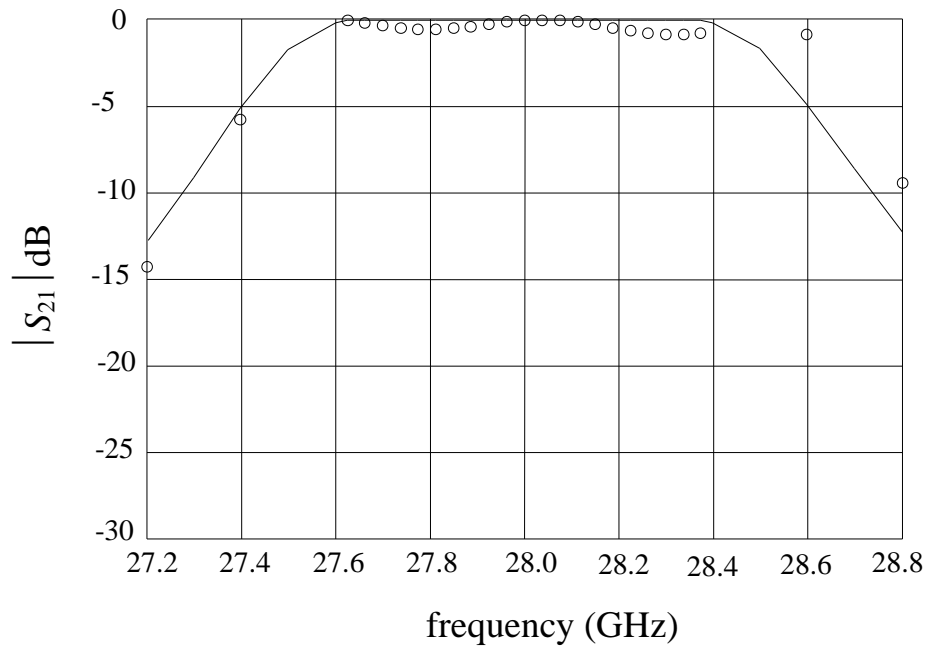
Fig. 15. The optimal coarse model response (—) and the fine model response (o) at the end of the second phase.

17
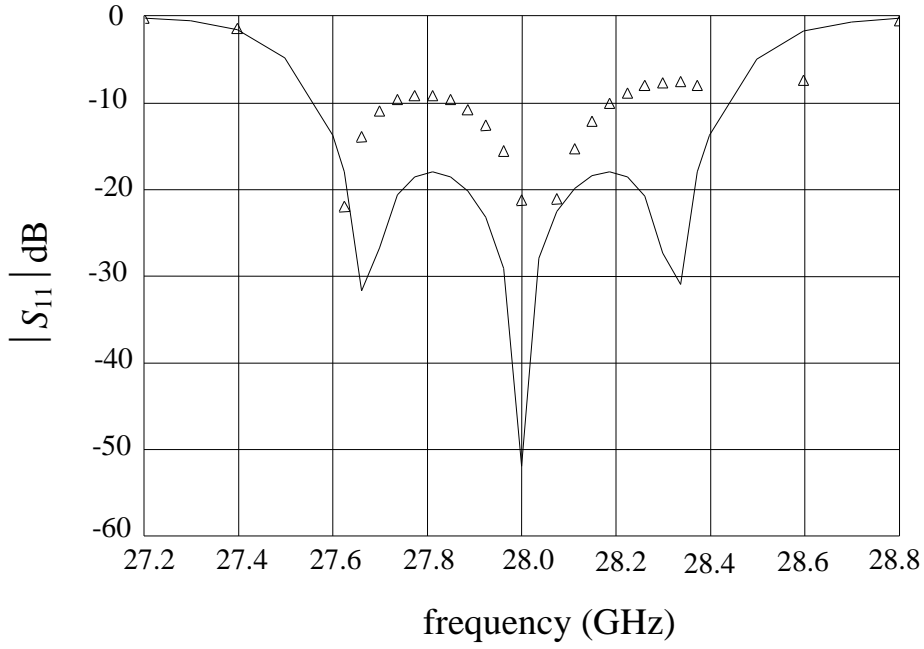
Fig. 16. The optimal coarse model response (——) and the fine model response (Δ) at the end of the second phase.
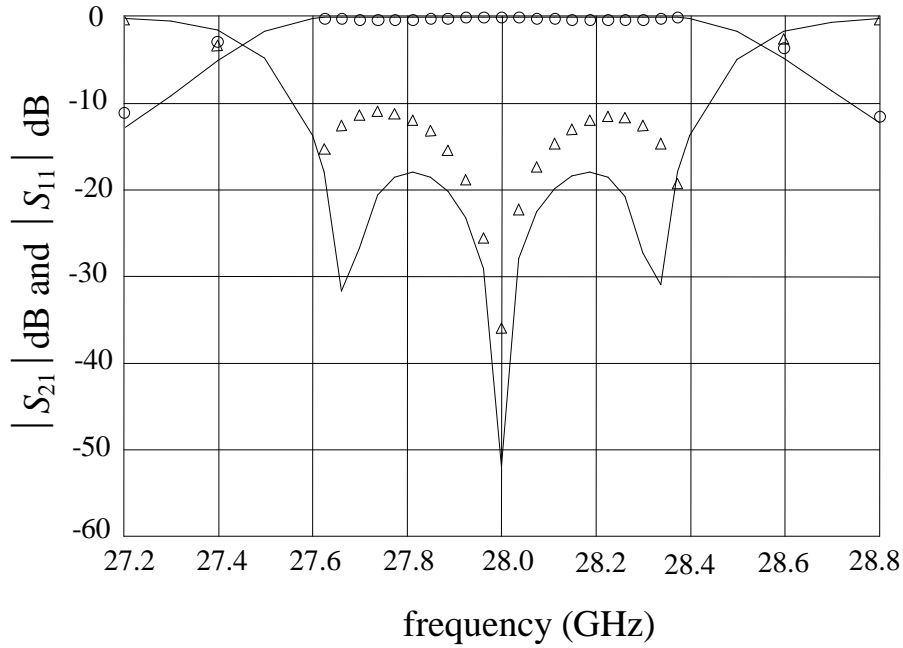
Fig. 17. The optimal coarse model response (——) (both $|S_{11}|$ and $|S_{21}|$) and the optimal fine model response ($|S_{21}|$ (o) and $|S_{11}|$ (Δ)).

18
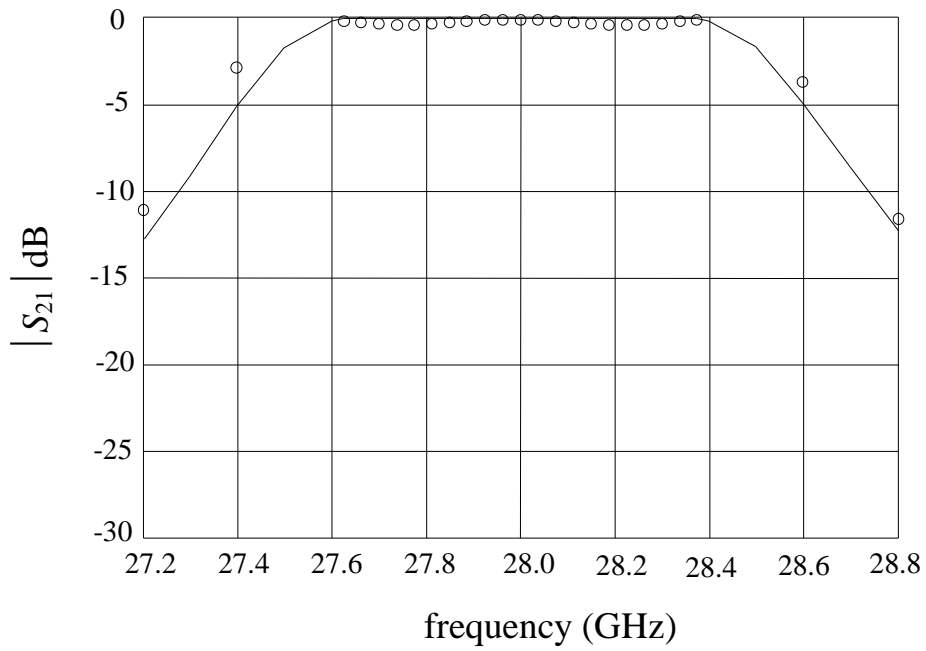
Fig. 18. The optimal coarse model response (—) and the optimal fine model response (o).
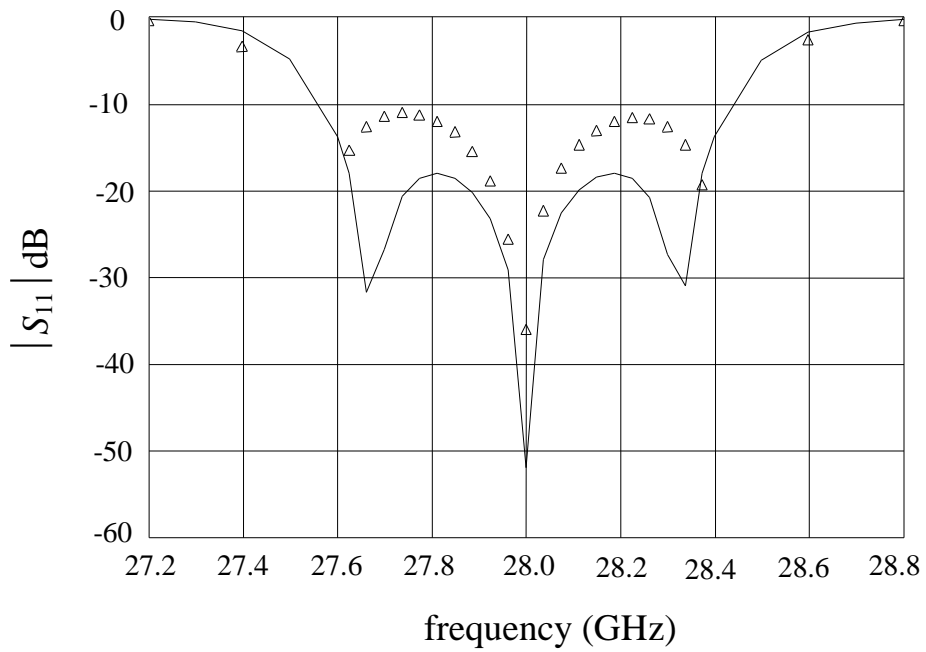
Fig. 19. The optimal coarse model response (—) and the optimal fine model response (Δ).

19
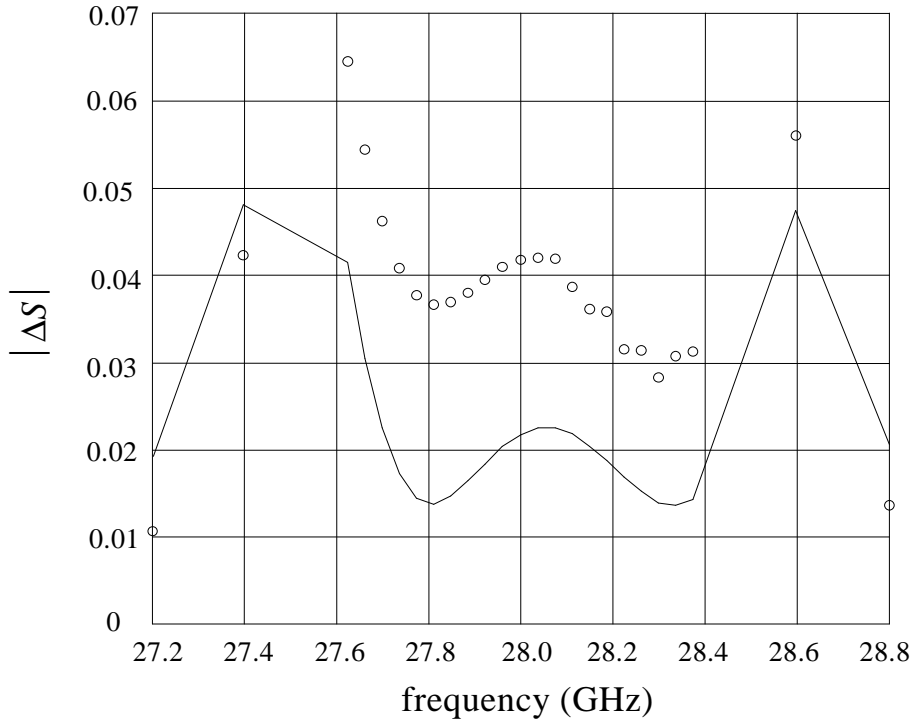
Fig. 20. The modulus of the difference of S_{21} (o) and S_{11} (—) at the point $\boldsymbol{x}''_{em}$ obtained using grid sizes in the *x*-direction of 0.5 mils and 0.25 mils.
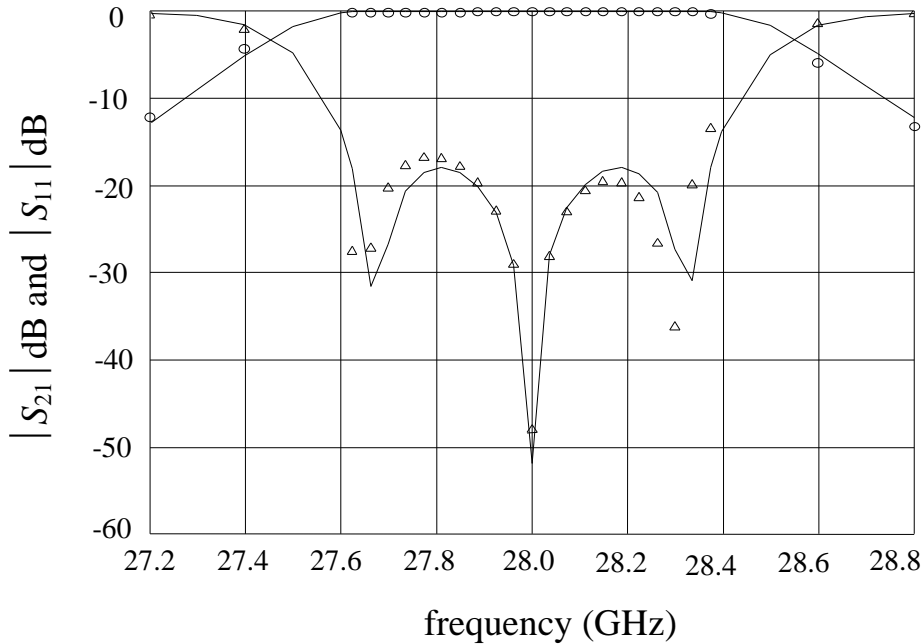
Fig. 21. The optimal coarse model response (—) (both $|S_{11}|$ and $|S_{21}|$) and the optimal fine model response ($|S_{21}|$ (o) and $|S_{11}|$ (△)) obtained using a grid size of 0.5 mils in the *x*-direction.
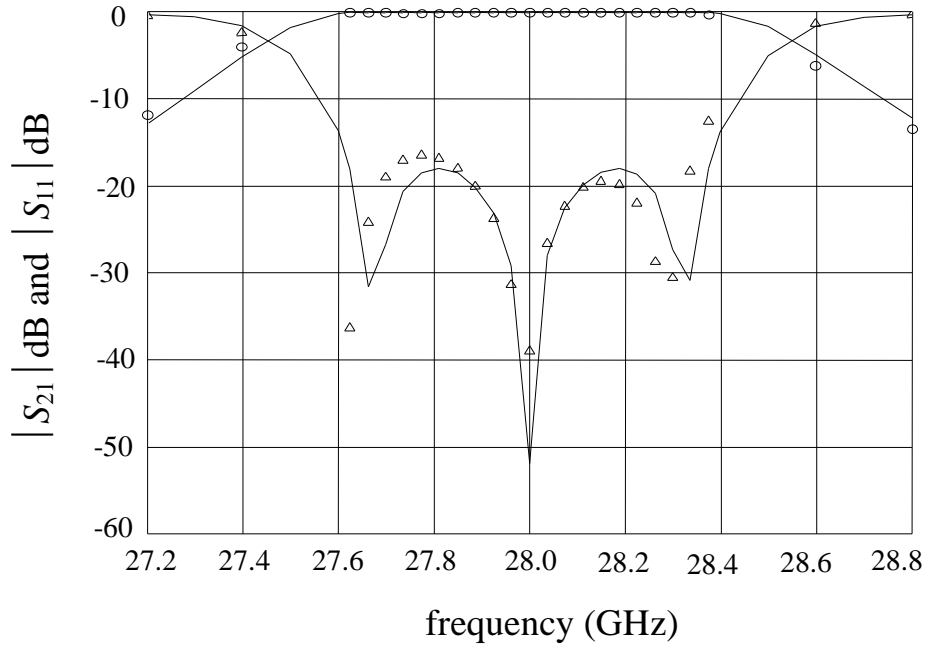
Fig. 22. The optimal coarse model response (—) (both $|S_{11}|$ and $|S_{21}|$) and the optimal fine model response ($|S_{21}|$ (o) and $|S_{11}|$ (Δ)) obtained using a grid size of 0.25 mils in the *x*-direction.
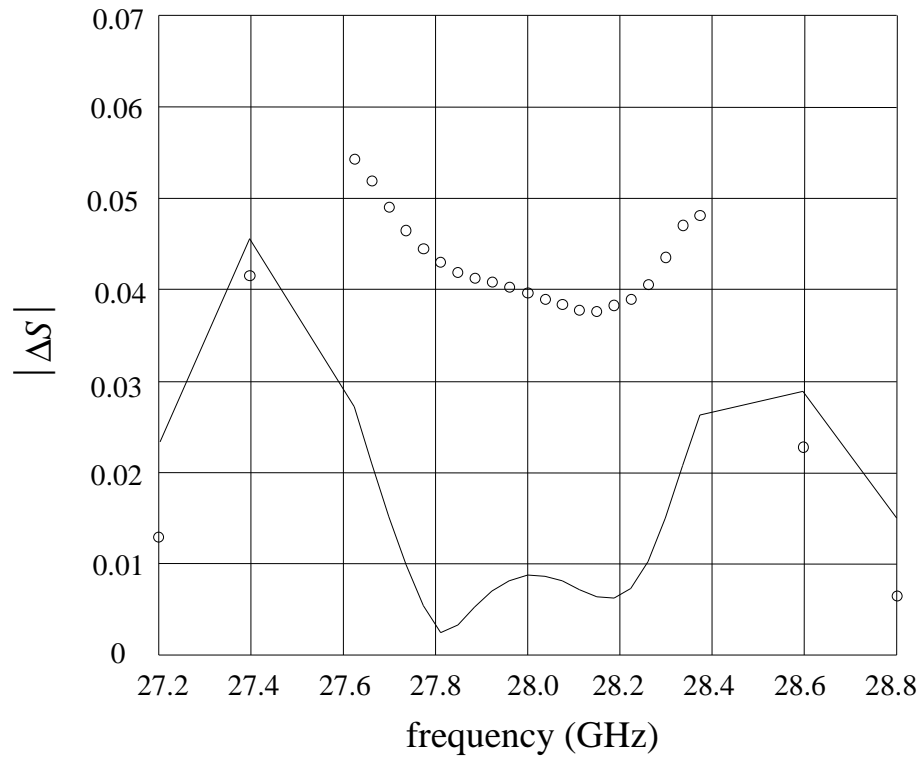
Fig. 23. The modulus of the difference of S_{21} (o) and S_{11} (—) at the minimax optimal design obtained using grid sizes in the *x*-direction of 0.5 mils and 0.25 mils.

APPENDIX A

```
! Example  nortel_filter.ckt
!  Wed Apr 21 14:50:07 1999. Minimax Optimizer. 24 Iterations. 00:00:52 CPU.
!  Wed Apr 21 14:53:58 1999. Minimax Optimizer. 22 Iterations. 00:00:40 CPU.
!  Wed Apr 21 15:06:29 1999. Minimax Optimizer. 20 Iterations. 00:00:37 CPU.

Expression
      MILMM=0.0254;            ! mil -> mm
      VL=2.99792458;          ! velocity of light,*1e+11 mm/s
      MU0=4*PI*1e-10;         ! H/mm
      EPS0=1/(4*PI*(VL^2)); ! pF/mm


      fmin=(27*1GHz);fmax=(29*1GHz);fstep=(0.005*1GHz);


      ER=2.2;
      WW=5;HSUB=10; ! mils

      S0=5; ! mil
      SC=5;
      SCL=S0+2*(SC+WW);
      D=S0+WW;

      Lin: ?77.1561?;
      LS1: ?42.5598?;
      LS2: ?8.81322?;
      LCLB: ?103.85?;
      LCLN: ?146.651?;


      WS=(WW*1mil);HS=(HSUB*1mil);
      QLS1=(0.25*LS1*1mil);
      QLS2=(0.25*LS2*1mil);
      HLS1=(0.5*LS1*1mil);
      HLS2=(0.5*LS2*1mil);
! effective dielectric constant, infinitesimally thin strip, non-dispersive
      WOH=WW/HSUB;
      A=1+LOG((WOH^4+(WOH/52)^2)/(WOH^4+0.432))/49+LOG(1+(WOH/18.1)^3)/18.7;
      B=0.564*((ER-0.9)/(ER+3))^0.053;
      EREF=0.5*(ER+1)+0.5*(ER-1)*((1+10/WOH)^(-A*B));
! mutual capacitance/unit length
      Z0: if (WOH <= 1) (60*LOG(8/WOH+WOH/4))
                      else (120*PI/(WOH+2.42-0.44/WOH+(1-1/WOH)^6));
      KL=120*PI/(Z0*WOH);
      KC=KL*(EREF/ER);

      CM0=(EPS0*ER/(4*PI))*KC*KL*(WOH^2)*LOG(1+(2*HSUB/S0)^2); ! pF/mm
      CMC=(EPS0*ER/(4*PI))*KC*KL*(WOH^2)*LOG(1+(2*HSUB/SC)^2); ! pF/mm

      C0S1=CM0*(HLS1*MILMM)*1e-3; ! nF -> HLS1
      C0S2=CM0*(HLS2*MILMM)*1e-3; ! nF -> HLS2
      CCS1=CMC*(HLS1*MILMM)*1e-3; ! nF -> HLS1
      CCS2=CMC*(HLS2*MILMM)*1e-3; ! nF -> HLS2
! mutual inductance/unit length
      LM0=0.1*LOG(1+(2*HSUB/D)^2);  ! nH/mm
      LM1=LM0*(HLS1*MILMM);         ! nH -> HLS1
      LM2=LM0*(HLS2*MILMM);         ! nH => HLS2
```

```
End

Model
      SUBCIRCUIT c_clines_1 1 2 3 4 5 6 7 8 0 {
            MSUB EPSR=ER H=HS;
            IND 2 21 L=(-LM1*1nH);
            MSCL 1 21 10 9 W=WS L=QLS1 S=(SC*1mil);
            MSCL 9 10 14 13 W=WS L=QLS1 S=(SC*1mil);
            MSCL 13 14 18 17 W=WS L=QLS1 S=(SC*1mil);
            MSCL 17 18 23 8 W=WS L=QLS1 S=(SC*1mil);
            IND 7 23 L=(-LM1*1nH);

            IND 3 22 L=(-LM1*1nH);
            MSCL 22 4 12 11 W=WS L=QLS1 S=(SC*1mil);
            MSCL 11 12 16 15 W=WS L=QLS1 S=(SC*1mil);
            MSCL 15 16 20 19 W=WS L=QLS1 S=(SC*1mil);
            MSCL 19 20 5 24 W=WS L=QLS1 S=(SC*1mil);
            IND 6 24 L=(-LM1*1nH);

            CAP 10 11 C=(C0S1*1nF);
            CAP 10 0 C=(-C0S1*1nF);
            CAP 11 0 C=(-C0S1*1nF);
            CAP 18 19 C=(C0S1*1nF);
            CAP 18 0 C=(-C0S1*1nF);
            CAP 19 0 C=(-C0S1*1nF);
                                    };
      SUBCIRCUIT c_clines_2 1 2 3 4 5 6 7 8 0 {
            MSUB EPSR=ER H=HS;
            IND 2 21 L=(-LM2*1nH);
            MSCL 1 21 10 9 W=WS L=QLS2 S=(SC*1mil);
            MSCL 9 10 14 13 W=WS L=QLS2 S=(SC*1mil);
            MSCL 13 14 18 17 W=WS L=QLS2 S=(SC*1mil);
            MSCL 17 18 23 8 W=WS L=QLS2 S=(SC*1mil);
            IND 7 23 L=(-LM2*1nH);

            IND 3 22 L=(-LM2*1nH);
            MSCL 22 4 12 11 W=WS L=QLS2 S=(SC*1mil);
            MSCL 11 12 16 15 W=WS L=QLS2 S=(SC*1mil);
            MSCL 15 16 20 19 W=WS L=QLS2 S=(SC*1mil);
            MSCL 19 20 5 24 W=WS L=QLS2 S=(SC*1mil);
            IND 6 24 L=(-LM2*1nH);

            CAP 10 11 C=(C0S2*1nF);
            CAP 10 0 C=(-C0S2*1nF);
            CAP 11 0 C=(-C0S2*1nF);
            CAP 18 19 C=(C0S2*1nF);
            CAP 18 0 C=(-C0S2*1nF);
            CAP 19 0 C=(-C0S2*1nF);
                                    };
      Lop=0.001*1mil;
      MSUB EPSR=ER H=HS;
      MSCL 1 2 5 4 W=WS L=(Lin*1mil) S=(S0*1mil);
      MOPEN 3 W=WS L=Lop;
      MOPEN 6 W=WS l=Lop;
      c_clines_1 3 4 5 6 7 8 9 10;
      MOPEN 8 W=WS L=Lop;
      MOPEN 9 W=WS L=Lop;
```

```
        MSCL 10 7 14 11 W=WS L=(LCLB*1mil) S=(SCL*1mil);
        MOPEN 12 W=WS L=Lop;
        MOPEN 13 W=WS L=Lop;
        c_clines_2 11 12 13 14 15 16 17 18;
        MOPEN 15 W=WS L=Lop;
        MOPEN 18 W=WS L=Lop;
        MSCL 17 16 21 20 W=WS L=(LCLN*1mil) S=(S0*1mil);
        MOPEN 19 W=WS L=Lop;
        MOPEN 22 W=WS L=Lop;
        c_clines_2 19 20 21 22 23 24 25 26;
        MOPEN 24 W=WS L=Lop;
        MOPEN 25 W=WS L=Lop;
        MSCL 26 23 30 27 W=WS L=(LCLB*1mil) S=(SCL*1mil);
        MOPEN 28 W=WS L=Lop;
        MOPEN 29 W=WS L=Lop;
        c_clines_1 27 28 29 30 31 32 33 34;
        MOPEN 31 W=WS L=Lop;
        MOPEN 34 W=WS L=Lop;
        MSCL 33 32 36 35 W=WS L=(Lin*1mil) S=(S0*1mil);

        PORT 1 2 R=100 X=0;
        PORT 35 36 R=100 X=0;

        CIRCUIT;

        MS21_DB: 20 * LOG10(MS21);
        MS11_DB: 20 * LOG10(MS11);
end

Sweep
   AC: FREQ: 27.2GHz 27.4GHz
           from 27.625GHz to 28.375GHz step=0.0375GHz
           28.6GHz 28.8GHz
           MS21 MS MS21_dB MS11_dB Lin LS1
        {Xsweep Title="Balanced filter, coarse model"
         Y=MS21.white Y_title="|S21|" Xmin=27.2 Xmax=28.8 Ymax=1 ! NXticks=15
         SPEC=(at 27.2, < 0.25).yellow &
              (from 27.625 to 28.375, > 0.987).yellow &
              (at 28.8, < 0.25).yellow};
end

Spec
   AC: FREQ: from 27.625GHz to 28.375GHz step=0.0375GHz MS21 > 0.987;
   AC: FREQ: 27.2GHz MS21 < 0.25;
   AC: FREQ: 28.8GHz MS21 < 0.25;
end

Control
      Allow_Neg_Parameters
end

Report
$%13.9f$ R=[ ${ $FREQ$  $MS21$ }$ ];
end
```